ELSEVIER

Contents lists available at ScienceDirect

# **Manufacturing Letters**

journal homepage: www.elsevier.com/locate/mfglet



# 3D printing of in-situ curing thermally insulated thermosets



Biran Wang <sup>a</sup>, Kristen F. Arias <sup>a</sup>, Zimeng Zhang <sup>a</sup>, Yuchen Liu <sup>a</sup>, Zhiyuan Jiang <sup>b</sup>, Hung-Jue Sue <sup>b</sup>, Nancy Currie-Gregg <sup>a</sup>, Stan Bouslog <sup>c</sup>, Zhijian (Z.J.) Pei <sup>a</sup>, Shiren Wang <sup>a,\*</sup>

- <sup>a</sup> Department of Industrial & Systems Engineering, Texas A&M University, College Station, TX 77843, USA
- <sup>b</sup> Polymer Technology Center, Department of Materials Science and Engineering, Texas A&M University, College Station, USA
- <sup>c</sup> NASA, Johnson Space Center, Engineering Directorate, Houston, TX 77058, USA

#### ARTICLE INFO

Article history:
Received 8 September 2018
Received in revised form 24 April 2019
Accepted 20 June 2019
Available online 21 June 2019

Keywords: Additive manufacturing 3D printing Thermosets Direct ink-writing (DIW)

#### ABSTRACT

This research reports additive manufacturing of in-situ curing thermosets using direct ink-writing (DIW) process. The investigation reveals the relationships between printing process parameters, such as extrusion pressure and operating temperature, and the resultant morphology and thermal conductivity. With the decrease of printing pressure from  $\sim\!125$  to  $\sim\!25$  mbar, crisscross structure appeared along with phonon boundary scattering effect which then causes  $\sim\!33\%$  reduction in thermal conductivity from  $\sim\!0.12~\text{Wm}^{-1}\text{K}^{-1}$  to  $\sim\!0.08~\text{Wm}^{-1}\text{K}^{-1}$ . The optimal cured temperature is found to be 75 °C, which yields thermal conductivity of  $\sim\!0.1~\text{Wm}^{-1}\text{K}^{-1}$  ( $\sim\!33\%$  decrease compared to the sample cured at 70 °C) without increase the roughness of the printed surface.

© 2019 Published by Elsevier Ltd on behalf of Society of Manufacturing Engineers (SME).

#### 1. Introduction

Thermoset materials are widely used in a variety of industries, such as aerospace, boating, and marine industry because of the exceptional specific strength and specific modulus. They are lightweight, inexpensive and easy to manufacture in comparison to other high-strength materials, like various metals and alloys [1]. However, the conventional manufacturing of thermoset materials including hand lay-up, filament winding processes and vacuum assisted resin transfer molding, etc., may take up to several hours to properly cure heating oligomers at elevated temperatures in a mold and retain their mechanical properties [2]. The oligomers are usually heated to more than 100 °C and undergo both external pressure and internal vacuum. Curing takes place in huge autoclaves that are bigger than the component [3]. In addition, it is difficult for conventional methods to manage change requests when the manufacturing process is already underway [4]. Particularly, it is very challenging for those conventional manufacturing processes to produce samples with complex geometry.

Additive manufacturing or 3D printing has been rapidly developed since the 1980s, and now is extensively used for numerous industries, such as biomedical engineering, energy devices, civil structures, and electronic systems [3,5]. It demonstrates many advantages over conventional methods, such as mold-free process,

material saving and freedom for design [4]. Particularly, additive manufacturing provides a promising way to thermosetting structures with complex geometry, which are difficult to produce using conventional methods. Among the various 3D printing techniques, the direct ink writing (DIW) has been proven to be especially effective in the thermoset fabrication because of the thermo-reactive characteristics and difficulty in the photocuring. DIW can continuously print thermosetting polymer ink layer-by-layer through a micro-nozzle, and allow it to solidify to create complex structures [6,7].

The type of ink used in DIW is especially important, and the ink composition and rheology should be tailored to achieve its printability. Ideal ink materials used in DIW usually possess some common rheological characteristics, such as shear-thinning behavior with a moderate yield stress to facilitate extrusion flow under shearing force [8] and excellent shape retention after deposition to maintain the printed geometry [9]. Most commonly used thermoset inks are epoxy based [8,6,10,11] and cyanate ester based [12]; however, they are usually printed in high viscosity and then cured after printing [13]. Frontal polymerization (FP) is a promising alternative curing strategy, in which a self-propagating exothermic reaction wave transforms liquid monomers to fully cured polymers [2], and thus offers a possibility for printing and curing in-situ. The experiment setup in this research is shown in Fig. 1.

Although some attempts have been made toward the mechanical properties of printed thermosetting materials [14–16], almost

<sup>\*</sup> Corresponding author.

E-mail address: s.wang@tamu.edu (S. Wang).

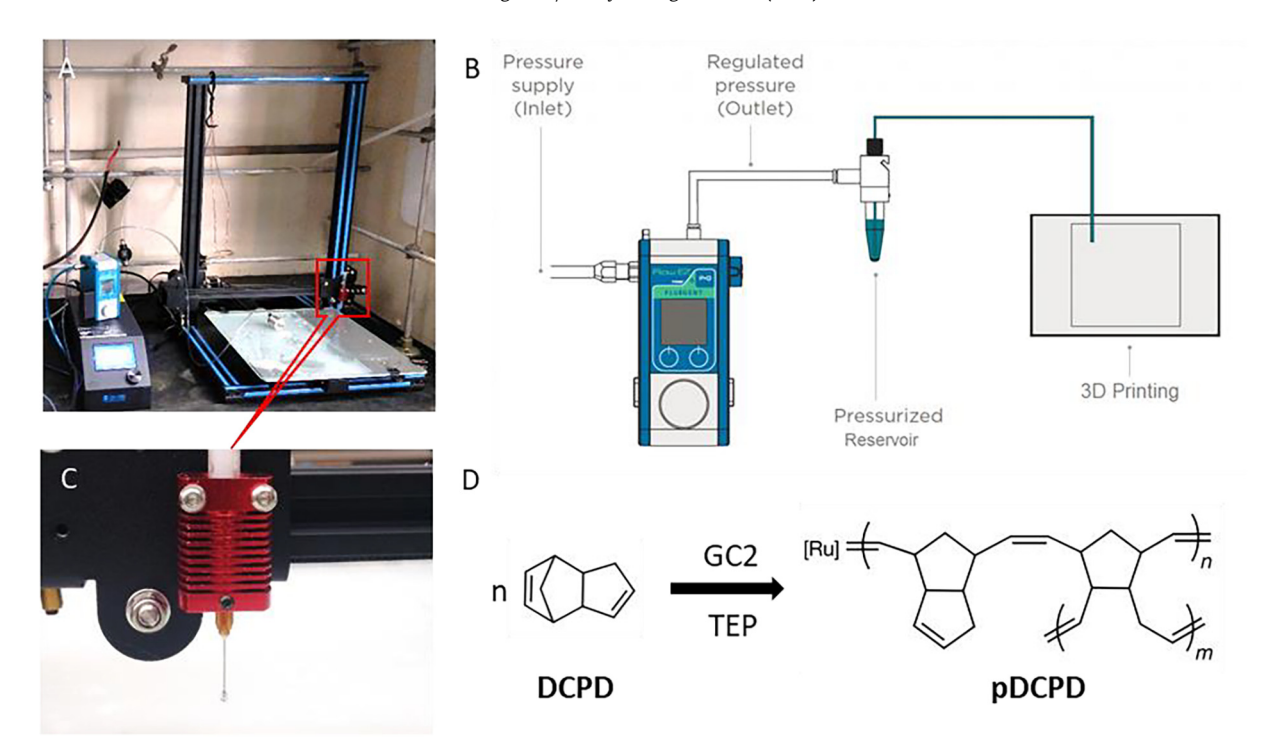


**Fig. 1.** Experiment Setup. (A): DIW 3D printer; (B): schematic setup of Flow-EZ pressure controller on DIW 3D printer; (C): adapted printer nozzle. (D): In-situ frontal polymerization of DCPD using a ruthenium catalyst GC2 (second generation Grubbs' catalyst) and an alkyl phosphite inhibitor (TEP).

no effort has been made to investigate the thermal properties of printed thermosetting materials. However, multi-functionality is of great interest in order to integrate the printed thermosetting materials into various systems. In this article, FP inks were developed according to the literature [2,17,18], and the effect of printing variables, mainly extrusion pressure, and operating temperature, on the resultant thermal properties of printed thermosetting materials is examined. The extrusion pressure and operating temperature are the two most basic parameters that significantly affect the DIW thermosets printing process. It is critical to understand how these parameters affect the thermal properties of printed products.

#### 2. Materials & methods

## 2.1. Materials

Dicyclopentadiene (DCPD), 5-ethylidene-2-norbornene (ENB), phenylcyclohexane (PC), and triethyl phosphite (TEP) were purchased from Sigma-Aldrich. Second-generation Grubbs' catalyst (GC2) was purchased from Chem-Impex International ("CII"). All the chemical ingredients were used as received without further purification or modification.

#### 2.2. Ink preparation

Ink preparation was adapted from the work by Robertson et al. [2], with slight modifications. The DCPD solution is the main ingredient of ink, it was prepared by adding 5 wt% ENB into melted DCPD solution at 40 °C under a chemical hood. ENB was used to depress the melting point of DCPD. The GC2 solution was prepared by dissolving 1 wt% GC2 powder into PC, which serves as the catalyst for frontal polymerization. TEP solution was prepared by mixing 10 vol% TEP into PC, which serves as the inhibitor. In a typical preparation, we add 6.4  $\mu$ l of TEP solution in 341  $\mu$ l of the GC2 solution, mix well, and then add into 5 g of DCPD solution. The final

molar proportion of ink is DCPD: GC2: TEP = 10,000:1:1. The final solutions degassed and then incubated for 2 h at room temperature.

#### 2.3. 3D printer

As shown in Fig. 2, DIW printer was refit from an FDM printer (Creality CR-10, SainSmart) that is capable of holding both extruders with a fine needle and a reservoir of ink. The reservoir of ink was placed in ice water in order to extend operating time. Connected to the reservoir is tubing leading to both the syringe in the nozzle and a pressure controller. The inner diameter of the nozzle was 0.3 mm, unless otherwise indicated. Pneumatic systems were purchased from Fluigent, the full scale of Flow-EZ pressure controller is between 0 and 7 bars. At least 5 samples were printed for each experiment.

#### 2.4. Characterization

The viscosity measurement was carried out on the Anton Paar Physica MCR-301 Rheometer, using the 50 mm cone-plate geometry. The viscosity is obtained from the shear rate sweep where the viscosity stables with the increasing shear rate.

In a homogenous body, thermal conductivity k can be determined as the product of thermal diffusivity, density, and specific heat capacity:

$$k = \alpha \rho C_p \tag{1}$$

where  $\alpha$  is thermal diffusivity,  $\rho$  is the density, and  $C_p$  is specific heat capacity.

The thermal conductivity and thermal diffusivity were measured and recorded by the thermal conductivity testing instrument (LFA 447 NanoFlash™, Netzsch) and its corresponding Nanoflash software using Laser Flash Method. The sample holders used in the apparatus are suitable for square samples with 10 mm side length. The samples were printed slightly larger than the sample holder, with a thickness of 1 mm. Briefly, the samples were firstly

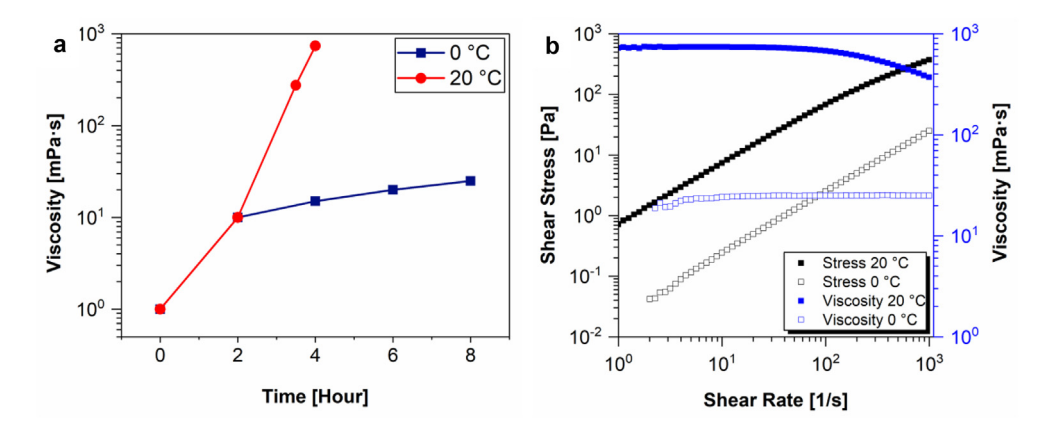


**Fig. 2.** Rheological properties of prepared ink. (a) The viscosity of prepared ink in different operating temperature. The inks were incubated at room temperature from hour 0 to hour 2. After that, they were stored in two temperature, 0 °C, and 20 °C. The viscosity of ink increased nearly 100 times within 2 h at 20 °C (red), while at 0 °C, it only slightly increased from 10 to 25 mPa.s, within 6 h (dark blue), (b) Rheological profile of the ink at 0 °C (hour 8) and 20 °C (hour 4). (For interpretation of the references to colour in this figure legend, the reader is referred to the web version of this article.)

cut off the edges to make them fit better inside the sample holder, then they were cleaned with isopropyl alcohol, and prior to the thermal diffusivity measurements, the front and back sides of the printed sample were coated with graphite 3 times to ensure an optimum emission/absorption capacity.

The sample density was measured by hydrostatic balance (64-15, Sartorius), following the vendor's instructions. It was determined by weighting the sample in air as well as in fluid. water was used as fluid in this study. By making use of the Archimedean Principle, the sample immersed in fluid is subjected to the force of buoyancy.

$$G = W - W_w \tag{2}$$

where G is buoyancy of the immersed sample, W is the weight of the sample (in air), and  $W_w$  is the weight of the solid in water. And the value of this buoyant force is the same as that of the weight of water displaced by the volume of the solid:  $G = \rho_w V$ . Therefore, the density of the sample can be obtained by

$$\rho = \frac{W}{V} = \frac{W}{G/\rho_w} = \frac{W}{W - W_w} \rho_w \tag{3}$$

The specific heat capacity was determined by the traditional three-run method using differential scanning calorimetry (DSC Q20, TA Instruments) according to ASTM E1269. Sapphire ( $\alpha$ -Al2O3) was used as the standard reference material. The heat flow calibration was performed using indium prior to every specific heat capacity measurement. The heat flow thermal curves of the empty sample holder, sapphire standard and sample can be used to calculate the specific heat capacity as follows:

$$C_p(s) = C_p(st) \cdot \frac{D_s \cdot W_{st}}{D_{st} \cdot W_s}$$
(4)

where  $C_p(s)$  is specific heat capacity of the sample,  $C_p(st)$  is specific heat capacity of the sapphire standard,  $D_s$  is vertical displacement between DSC thermal curves of the empty sample holder and the specimen at a given temperature,  $D_{st}$  is vertical displacement between DSC thermal curves of the empty specimen holder and the sapphire standard at a given temperature,  $W_s$  is mass of sample,  $W_{st}$  is mass of sapphire standard.

The surface morphology of 3D printed samples was measured using an Olympus CX51 microscope. The surfaces topography is rated using the optical interferometer (Model ZYGO/14-21-75092) using a magnification of  $\times 5$ .

#### 2.5. Software

The initial design of thermoset samples was designed by Solid-Works. Slic3r was the software that translates this blueprint into G Code, which is the programming language 3D printers read. The patterns, printing speed and infill percentages were also modified by Slic3r. 3D printer itself was controlled by Repetier Host. It can send the sliced G code to the printer, to control the X, Y and Z movement of the nozzle, the cooling fans, bed temperature, etc.

### 3. Results and discussion

FP was firstly reported half a century ago [19], and this autoactivation process produces a propagating reaction wave that rapidly transforms the available monomer into polymer. It has been used to synthesize a variety of polymeric materials [20-22]; however, most of these materials used in FP are unsuitable for highperformance applications [2]. DCPD resins have been widely used owing to its excellent physical and mechanical properties. FP of DCPD was performed for the first time by Mariani et al. [23] using the first generation Grubbs' catalyst and demonstrated high front temperatures and velocities via varying the monomer/catalyst ratio. However, it suffered from short pot-life, only a few seconds, and thus the polymerization mixture had to be immediately cooled down under the DCPD melting temperature to avoid spontaneous polymerization [23]. Robertson et al. found that the alkyl phosphite inhibitors substantially extend the liquid-processing window for FP of DCPD [17].

## 3.1. Ink characterization

In this article, TEP was used as phosphite-inhibitor for FP of DCPD. The printability of prepared inks was firstly investigated, mainly include the GE2/TEP ratio, rheological properties of the ink, and pot life. The different catalyst/inhibitor GE2/TEP ratios had a prominent effect on the printability of ink, three different ratios, 1:0.5, 1:1, 1:2, have been prepared. The results showed that 1:0.5 ratio was not enough to inhibit the reaction kinetics, DCPD solution solidified in a few minutes after adding the GE2/TEP (1:0.5) solution. While the DCPD solution didn't cure after mixing with the GE2/TEP (1:2) solution. We finally obtained the optimal catalyst/inhibitor ratio at 1:1. Furthermore, as shown in Fig. 2c, the rheological profile of ink showed that the viscosity increased nearly 100 times within 2 h at room temperature (red), while at 0 °C, it only slightly increased from 10 to 25 mPa.s within 6 h (dark

blue), therefore, the ink must be kept at cool temperatures in order to extend its pot life. In fact, the pot life of ink could be extended up to 24 h if we store it at 0 °C. Fig. 2d compared the rheological profile of prepared inks at 0 °C after 8 h and at 20 °C after 4 h. The ink at 20 °C showed shear thinning behavior, while the one at 0 °C showed Newtonian fluid characteristics. For all the thermal property studies, we always keep the ink reservoir in ice water to extend its pot life.

DCPD-based thermosetting materials demonstrated desired processing characteristics and low thermal conductivity [24], and thus they are very promising candidates for many thermal insulation applications [25]. Thermal conductivity is the main characteristic of a materials' thermal property, and it describes the ability to conduct heat. As described in Eq. (1), to precisely determine the thermal conductivity, we measured all the 3 parameters  $\alpha$ ,  $\rho$ ,  $C_p$  of each printed sample. The result shows that there is no significant difference in the density of printed samples, and they all around 1.2 g/cm³. In contrast, the specific heat capacity of printed samples is quite different as shown in Figs. S1 and S2. We examined the thermal transport as a function of printing pressure and temperature and the results are shown in Figs. 3 and 4.

#### 3.2. Influence of extrusion pressure

he applied pressure is a very important factor in DIW printing because it can significantly affect the printing speeds, the morphology and the thickness of printed samples. If the applied pressure is too low, the DIW printing ink would be discontinuous; while the applied pressure is too high, too much ink would spread on substrate, and this may damage the nozzles because the printed ink may be solidified and choke the flow. We finally found out that

pressure between 0 and 200 mbar is good for the printability and further studied.

As shown in Fig. 3a and c, the thickness of printed samples increase as the pressure increases. The thermal properties of printed samples have been greatly influenced by the applied pressure, as shown in Fig. 3b, the thermal conductivity of printed samples decreased as the pressure was decreased. The reduction of thermal conductivity is due to that at a lower pressure (25 and 50 mbars), there are clearly printed lines and interspaces, while at higher pressure (above 75 mbar), no more visible writing lines can be observed, only the thickness is increased, as shown in Fig. 3d. These visible crisscross lines and interspaces at lower pressure conditions cause a strong phonon–boundary scattering effect, therefore reduce the thermal conductivity of printed samples.

## 3.3. Influence of operating temperature

The initial temperature is also a very important factor for FP. The increase in the initial temperature increased the front temperature, which leads to more soluble oligomers and a higher degree of crosslinking [26]. The printability of the DIW printer is very sensitive to the initial temperature, aka the bed temperature. If the initial temperature is too low, the FP cannot be initiated right away. Conversely, if it's too high, the FP reaction may be too quick to block the extruder. In our experiment, the temperature of the substrate bed serves as the initial temperature for FP of DCPD inks was tested for the best performance of the printer was ranging from 70 °C to 90 °C.

We also determined the density, specific heat capacity, the thermal diffusivity of printed samples at different initial operating temperature from 70 °C to 90 °C to finally determine their thermal conductivity. Strangely, the thermal conductivity wasn't affected

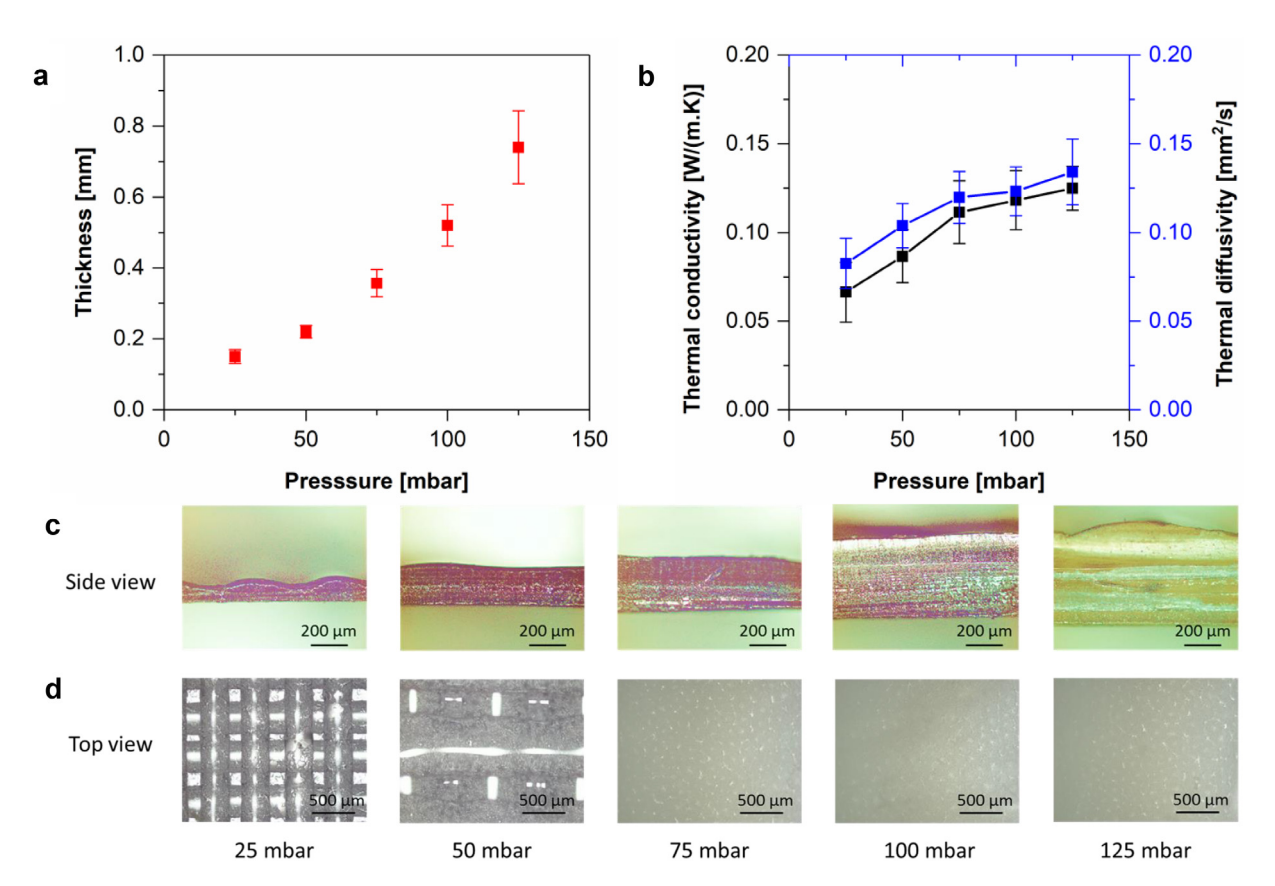
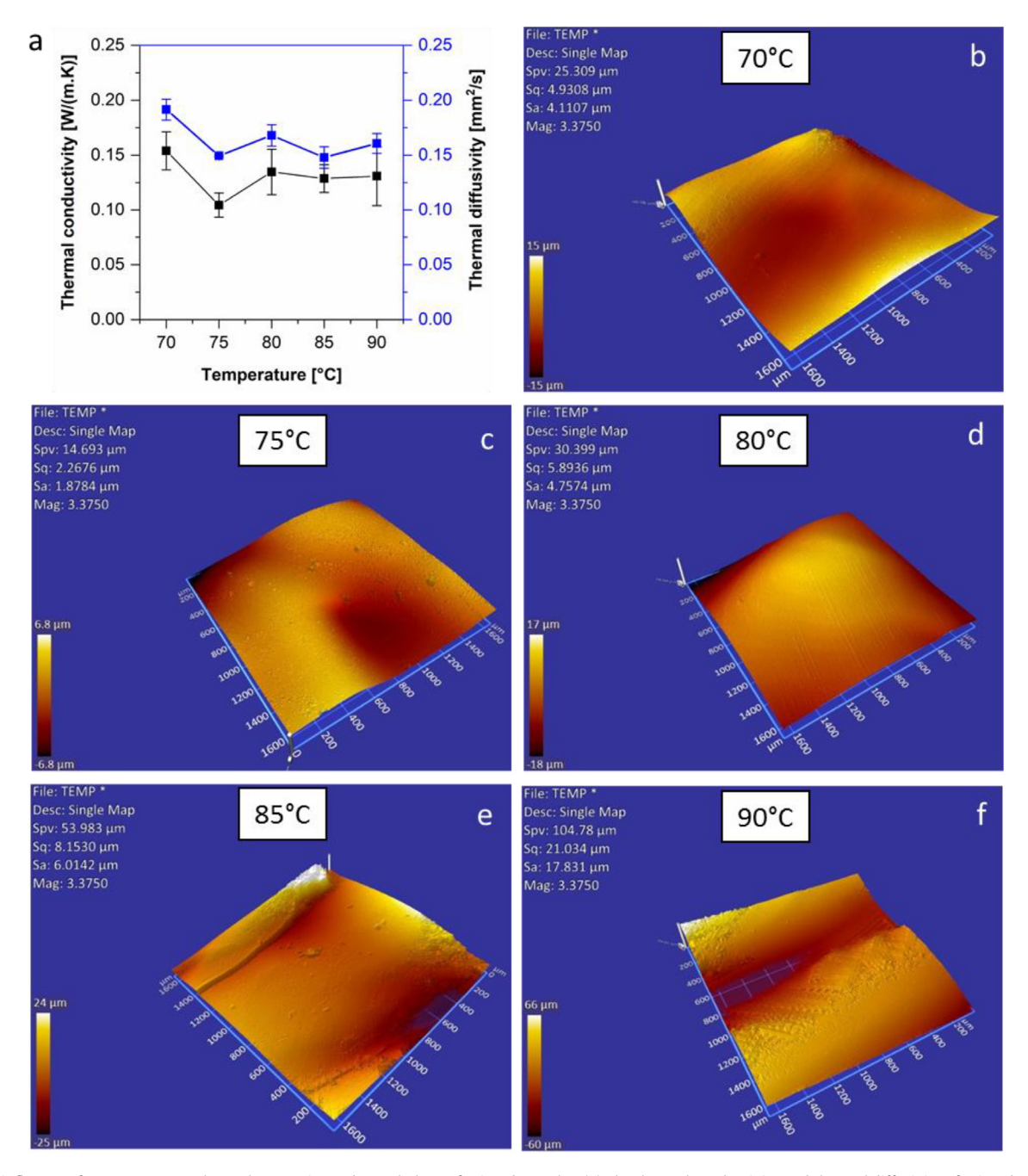


Fig. 3. The influence of pressure on the thickness and thermal properties of printed samples (a and b). The thickness (a), thermal conductivity and thermal diffusivity (b) of printed samples in the function of applied pressure. The side view (c) and top view (d) of printed samples under different pressure conditions.



**Fig. 4.** The influence of temperature on thermal properties and morphology of printed samples. (a) The thermal conductivity and thermal diffusivity of printed samples in the function of initial temperature, (b–f) the morphology of printed samples at different temperatures.

by the initial temperature, and no significant variation of thermal conductivity has been observed as the temperature was increased. As shown in Fig. 4a, the thermal conductivities of thermoset at five different temperatures were all around 0.1–0.15 W/(m.K). The morphology of printed samples, however, is quite different. We observed a glass-transition temperature Tg around 83 °C. When the bed temperature is below Tg, the printed samples showed a liquid form, and then solidified a few seconds to a few minutes later, depending on the bed temperature, so basically, the printed lines didn't maintain their shapes, as they are still in liquid form, they could spread around to have a smooth surface. This is due to different frontal velocity induced at different print bed temperature with the coordination of printing speed. According to [2], frontal velocity increases with increased temperature. When the printing

speed is slower than the frontal velocity, inks were solidified instantly right after the extrusion, resulted in a less smooth surface. The surface morphology of printed samples under different curing temperature is from 70 °C to 90 °C at an interval of 5 °C shown in Fig. 4b–f, respectively. Fig. 4b–d were printed below 83 °C, the surface of printed samples is much smoother than the Fig. 4e and f, which were printed above 83 °C, we can visibly see the roughness on the surface of the sample as they cured in situ.

# 4. Conclusions

In conclusion, we demonstrated an advanced in situ 3D printing techniques for the additive manufacture of high-performance thermosetting materials. By controlling the extrusion pressure and operating temperature, the morphology and the thermal conductivity were successfully tuned. The crisscross structure was obtained at lower pressure while no obvious pattern was formed at a pressure higher than 75 mbar. There is a  $\sim$ 33% reduction in thermal conductivity at a low extrusion pressure of 25 mbar compared to the elevated pressure of 75 mbar due to phonon boundary scattering. The lowest thermal conductivity of 0.1 Wm<sup>-1</sup> K<sup>-1</sup> was obtained when the curing temperature is 75 °C. This achieves tunable thermal properties through alternating printing process parameters, which exhibits the great potential of 3D printing thermosetting materials in aerospace applications. Considering the wide range of application of thermosetting materials in aerospace, the application of the presented approach and the specific findings will substantially lead to a number of new research ideas and industrial opportunities, such as innovative FP materials development, large-scale aircraft production, in situ 3D printing in space, etc.

#### **Declaration of Competing Interest**

None.

#### Acknowledgments

We are grateful to the Texas A&M University and TEES startup funds and support, and NSF (CMMI 1634858). The undergraduate research assistant involved in this research activity is supported by the National Science Foundation under REU Site Grant (# EEC 1757882).

## Appendix A. Supplementary data

Supplementary data to this article can be found online at https://doi.org/10.1016/j.mfglet.2019.06.001.

### References

- Rodriguez JN, Zhu C, Duoss EB, Wilson TS, Spadaccini CM, Lewicki JP. Shapemorphing composites with designed micro-architectures. Sci Rep 2016;6(1).
- [2] Robertson ID, Yourdkhani M, Centellas PJ, Aw JE, Ivanoff DG, Goli E, et al. Rapid energy-efficient manufacturing of polymers and composites via frontal polymerization. Nature 2018;557(7704):223–7.
- [3] Kuang X, Zhao Z, Chen K, Fang D, Kang G, Qi HJ. High-speed 3D printing of high-performance thermosetting polymers via two-stage curing. Macromol. Rapid Commun. 2018;39(7):1700809.
- [4] Fette M, Sander P, Wulfsberg J, Zierk H, Herrmann A, Stoess N. Optimized and cost-efficient compression molds manufactured by selective laser melting for the production of thermoset fiber reinforced plastic aircraft components. Procedia CIRP 2015;35:25–30.

- [5] Hao W, Liu Y, Zhou H, Chen H, Fang D. Preparation and characterization of 3D printed continuous carbon fiber reinforced thermosetting composites. Polym Test 2018:65:29–34.
- [6] Lewicki JP, Rodriguez JN, Zhu C, Worsley MA, Wu AS, Kanarska Y, et al. 3D-Printing of meso-structurally ordered carbon fiber/polymer composites with unprecedented orthotropic physical properties. Sci Rep 2017;7:43401.
- [7] Lewis JA. Direct ink writing of 3D functional materials. Adv Funct Mater 2006;16(17):2193–204.
- [8] Compton BG, Lewis JA. 3D-printing of lightweight cellular composites. Adv Mater 2014;26(34):5930–5.
- [9] Zhu C, Smay JE. Catenary shape evolution of spanning structures in directwrite assembly of colloidal gels. J Mater Process Technol 2012;212(3):727–33.
- [10] Compton BG, Kemp JW, Novikov TV, Pack RC, Nlebedim CI, Duty CE, et al. Direct-write 3D printing of NdFeB bonded magnets. Mater Manuf Process 2018;33(1):109–13.
- [11] Hmeidat NS, Kemp JW, Compton BG. High-strength epoxy nanocomposites for 3D printing. Compos Sci Technol 2018;160:9–20.
- [12] Chandrasekaran S, Duoss EB, Worsley MA, Lewicki JP. 3D Printing of high performance cyanate ester thermoset polymers. J Mater Chem A 2018;6 (3):853–8.
- [13] Ligon SC, Liska R, Stampfl J, Gurr M, Mülhaupt R. Polymers for 3D printing and customized additive manufacturing. Chem Rev 2017;117(15):10212–90.
- [14] Naranjo-Lozada J, Ahuett-Garza H, Orta-Castañón P, Verbeeten WMH, Sáiz-González D. Tensile properties and failure behavior of chopped and continuous carbon fiber composites produced by additive manufacturing. Addit Manuf 2019;26:227–41.
- [15] Melenka GW, Cheung BKO, Schofield JS, Dawson MR, Carey JP. Evaluation and prediction of the tensile properties of continuous fiber-reinforced 3D printed structures. Compos Struct 2016;153:866–75.
- [16] Spackman CC, Frank CR, Picha KC, Samuel J. 3D printing of fiber-reinforced soft composites: process study and material characterization. J Manuf Process 2016;23:296–305.
- [17] Robertson ID, Dean LM, Rudebusch GE, Sottos NR, White SR, Moore JS. Alkyl phosphite inhibitors for frontal ring-opening metathesis polymerization greatly increase pot life. ACS Macro Lett 2017;6(6):609-12.
- [18] Robertson ID, Pruitt EL, Moore JS. Frontal ring-opening metathesis polymerization of exo-dicyclopentadiene for low catalyst loadings. ACS Macro Lett 2016;5(5):593–6.
- [19] Chechilo NM, Khvilivitskii RYa, Enikolopyan NS. Propagation of the polymerization reaction. Dokl Akad Nauk SSSR 1972;204(5):1180–1.
- [20] Nuvoli D, Alzari V, Pojman JA, Sanna V, Ruiu A, Sanna D, et al. Synthesis and characterization of functionally gradient materials obtained by frontal polymerization. ACS Appl Mater Interfaces 2015;7(6):3600–6.
- [21] Guo X, Wang C-F, Fang Y, Chen L, Chen S. Fast synthesis of versatile nanocrystal-embedded hydrogels toward the sensing of heavy metal ions and organoamines. J Mater Chem 2011;21(4):1124–9.
- [22] Robertson ID, Hernandez HL, White SR, Moore JS. Rapid stiffening of a microfluidic endoskeleton via frontal polymerization. ACS Appl Mater Interfaces 2014;6(21):18469–74.
- [23] Mariani A, Fiori S, Chekanov Y, Pojman JA. Frontal ring-opening metathesis polymerization of dicyclopentadiene. Macromolecules 2001;34(19):6539–41.
- [24] Le Gac PY, Choqueuse D, Paris M, Recher G, Zimmer C, Melot D. Durability of polydicyclopentadiene under high temperature, high pressure and seawater (Offshore Oil Production Conditions), Polym Degrad Stab 2013;98(3):809–17.
- [25] Lee JK, Gould GL. Polydicyclopentadiene based aerogel: a new insulation material. J Sol-Gel Sci Technol 2007;44(1):29–40.
- [26] Yan Q-Z, Zhang W-F, Lu G-D, Su X-T, Ge C-C. Frontal polymerization synthesis of starch-grafted hydrogels: effect of temperature and tube size on propagating front and properties of hydrogels. Chem – Eur J 2006;12 (12):3303-9.